Stimuli-responsive polymeric prodrug-based nanomedicine delivering nifuroxazide and doxorubicin against primary breast cancer and pulmonary metastasis

Lei Luo, Fanshu Xu, Huilan Peng, Yonghuang Luo, Xiaohe Tian, Giuseppe Battaglia, Hu Zhang, Qiyong Gong, Zhongwei Gu, Kui Luo

PII: S0168-3659(19)30736-9

DOI: https://doi.org/10.1016/j.jconrel.2019.12.017

Reference: COREL 10060

To appear in: *Journal of Controlled Release*

Received date: 31 October 2019

Revised date: 8 December 2019

Accepted date: 11 December 2019

Please cite this article as: L. Luo, F. Xu, H. Peng, et al., Stimuli-responsive polymeric prodrug-based nanomedicine delivering nifuroxazide and doxorubicin against primary breast cancer and pulmonary metastasis, *Journal of Controlled Release* (2019), https://doi.org/10.1016/j.jconrel.2019.12.017

Stimuli-responsive polymeric prodrug-based nanomedicine delivering nifuroxazide and doxorubicin against primary breast cancer and pulmonary metastasis

Lei Luo [a,*], Fanshu Xu [a], Huilan Peng [a], Yonghuang Luo [a], Xiaohe Tian [c], Giuseppe Battaglia [e], Hu Zhang [d], Qiyong Gong [b], Zhongwei Gu [b], Kui Luo [b,*]

[a] Key Laboratory of Luminescent and Real-Time Analytical Chemistry (Southwest University), Ministry of Education, College of Pharmaceutical Sciences, Southwest University, Chongqing 400715, PR China

[b] Huaxi MR Research Center (HMRRC), Department of Radiology, West China Hospital, Functional and molecular imaging Key Laboratory of Sichuan Province, and National Engineering Research Center for Biomaterials, Sichuan University, Chengdu 610041, China

[c] Department of Chemistry, Key Laboratory of Functional Inorganic Material Chemistry of Anhui Province, Anhui University, Hefei 230039, P. R. China.

[d] Amgen Bioprocessing Centre, Keck Graduate Institute, Claremont, CA 91711, USA

[e] Department of Chemistry, and Department of Chemical Engineering, University College London, UK

*Corresponding authors.

E–mail: luokui@scu.edu.cn (Kui); drluolei@swu.edu.cn (Lei)

ABSTRACT:

Functionalized drug delivery systems against malignant lung metastasis of breast cancer have been extensively studied, while metastasis remains a challenging issue. We propose a new strategy to achieve eradication of primary breast cancer cells and inhibition of pulmonary metastasis. A cathepsin B/pH dual-sensitive block copolymer with a molecular weight of 92 kDa was synthesized to conjugate with doxorubicin (DOX). The copolymer-DOX was further loaded with nifuroxazide (NFX) to self-assemble co-prodrug-loaded micelles (CLM). CLM displayed a drug release pattern in response to pH/enzyme dual stimuli and was enzymatically biodegradable. CLM was demonstrated to reduce viability and inhibit migration and invasion of 4T1 murine breast cancer cells in vitro. After i.v. injection of CLM, its nanoscale size and stimuli-responsiveness facilitated delivery of drugs to the tumor site in mice. Enhanced anti-tumor efficacy and great anti-metastatic effects were found in both orthotropic and lung metastasis 4T1 breast cancer mice models. Meanwhile, histological immunofluorescence and immunohistochemical analyses revealed a high level of apoptosis, suppressed expression of matrix metalloproteinases and reduction in MDSCs infiltration, and all these contributed to inhibit pulmonary metastasis. CLM may be explored as a potential nanomedicine against breast cancer metastasis.

Keywords: polymeric prodrug; stimuli-responsive; drug delivery; breast metastasis; controlled release

1. Introduction

Breast cancer, a common type of malignant disease, causes high mortality due to its metastasis, especial metastasis in lungs [1-3]. Currently, chemotherapy and radiotherapy are often applied after surgical removal of visible tumors. However, conventional chemotherapies have severe side effects and limited efficacy against metastasis [4]. To address these challenges, great efforts have been devoted to developing nano-sized drug delivery systems (DDS) such as liposomes and micelles for loading chemotherapy agents [5, 6]. DDS have been reported to hold great advantages, including improved drug solubility, prolonged blood circulation, passive delivery of chemotherapy drugs to tumors via the enhanced permeation and retention (EPR) effect, and simultaneous delivery of multiple agents [7-10]. However, most DDS are only able to inhibit growth of primary tumors, but not effective in preventing metastasis. It is crucial to precisely deliver a drug or multiple agents into tumor tissues for not only eradicating primary tumor cells but also inhibiting metastasis.

Polymeric prodrug-based DDS integrate the advantages of prodrugs and nanoparticles. The prodrug could be pharmacologically inactive in vitro and is readily converted into its parent drug in vivo [11]. Such a DDS is designed and prepared for improving drug loading, enhancing stability, and reducing side effects. Moreover, polymeric prodrug-based DDS could achieve great cellular uptake efficiency through endocytosis, in which nano-sized DDS can detach a small piece of the bilayer membrane of cancer cells and the piece wraps the DDS into the cells [12]. To further improve the drug delivery targeting, stimuli-responsive polymeric prodrugs are constructed and the stimuli include pH [13], glutathione (GSH) [14], reactive oxygen species (ROS) [15], enzymes [16] and light [17, 18]. Tumors have been demonstrated to have an acidic pH value ranging from 5.7 to 6.8 in the extracellular environment

and a lower pH in the range 4.5-5.5 in late endosomes and lysosomes [19]. Instead of synthesizing ionizable polymers to respond in a low pH, a novel approach by building an acid-labile linker such as a hydrazone bond between drug molecules and polymeric carriers is developed for specifically triggering drug release in the acidic tumor environment. This could maintain the stability and improve the safety of prodrug molecules at a physiological pH, but precisely convert the prodrugs into parent drugs at the tumor site [20, 21]. Additionally, enzyme-sensitive prodrugs could precisely release drugs at the tumor site through hydrolyzing the amide bonds of protein molecules by specific proteases. Cathepsin B (CB) is an important member of the papain cysteine protease family and it is often highly expressed in tumor cells. Among many peptides that are hydrolyzed by CB, glycylphenylalanyl-leucyl-glycine (GFLG) is often applied as a link between drugs and carrier materials [22, 23]. The linker can be cleaved by CB in lysosomes, and anticancer drugs are effectively released at the tumor site, thus decreasing the side effects of these drugs.

In this study, doxorubicin (DOX) was selected as a model anti-cancer drug that has been widely used to treat cancers. However, one main disadvantage of DOX is its cardiotoxicity, which limits its maximum tolerant dose. Herein, DOX was conjugated to a hydroxypropyl methacrylate (HPMA) and oligo-(ethylene glycol) methacrylate (OEGMA) copolymer via a pH sensitive linker, and the backbone of the polymeric carrier was constructed with enzyme-sensitive peptide GFLG to build a prodrug polymer. Moreover, a hydrophobic anti-metastasis agent, nifuroxazide (NFX), was non-covalently encapsulated into the prodrug polymer to form DOX/NFX co-loaded micelles (CLM). NFX has been demonstrated to block breast cancer cell migration and invasion without significant cytotoxicity [24]. Importantly, NFX enhances antitumor immunity and inhibit lung metastasis by reducing the number of myeloid

derived suppressor cells (MDSCs) in lungs [25]. Therefore, the combination therapy was expected to eliminate solid tumor and inhibit metastasis after accurately delivering both agents to the tumor sites by polymeric prodrug micelles. CLM was characterized by transmission electronic microscope (TEM), dynamic light scattering (DLS), and ultraviolet (UV) spectrometry. The cytotoxicity, the inhibitory effect on metastasis and invasion of CLM were evaluated against 4T1 murine breast cancer cells. Murine orthotropic and lung metastasis breast cancer models were established to quantify the anti-tumor and anti-metastasis efficacy of CLM. The prodrug micelles have been found to improve solubility of DOX and NFX, controlled release drugs at the sites of action, thus offering a novel chemotherapy recipe of NFX and DOX against breast cancer and lung metastasis.

2. Experimental section

2.1. Reagents and methods

The information about chemical reagents for preparation of the polymeric prodrug and the methods for characterization of the prodrug was provided in the Supporting Information. Nifuroxazide was purchased from Aladdin (China). VA044, papain, and cathepsin B were purchased from Sigma Aldrich (USA). Regenerated cellulose dialysis membrane (Spectra/Por 6, MWCO = 3,500 Da) was supplied by Thermo Fisher Scientific (USA). Size distribution and Zeta potential were determined by a Zeta-sizer (Malvern Instruments, UK). The UV-VIS spectrum was recorded on a UV-6100 spectrophotometer (Shanghai Mapada Instruments Co., Ltd, China). The critical micelle concentration (CMC) was measured by a F-7000 fluorescence spectrophotometer (Hitachi, Japan). JEM1200EX transmission electron microscopy (JEOL, Japan) was used for morphology characterization and a microplate reader (Biotek ELx800, Gene Co., Ltd, USA) for cell viability analysis.

2.2. Cells and Animals

The 4T1 murine breast cancer cell line was obtained from the Chinese Academy of Science Cell Bank for Type Culture Collection (China). Cells were propagated in the DMEM media containing 10% heat-inactivated fetal bovine serum (FBS, Hyclone, Logan, UT, USA) at 5% CO_2 at 37 °C. Female BALB/c mice (20 ± 2 g, 6-8 weeks of age) were purchased from the Experimental Animal Center, Chongqing Medical University. All animal experiments were approved by the Institutional Animal Care and Treatment Committee of Southwest University.

2.3. Synthesis

The monomers HPMA (869 mg, 6.08 mmol), MA-NHNHBoc (1.10 g, 4.05 mmol) and the functionalized peptide CTA-GFLGKGLFG-CTA (70 mg, 49.2 μmol) were incubated in a vial and protected in an argon atmosphere. 6 mL solution of methanol and water (3/1, v/v) with VA044 (10.6 mg, 32.7 μmol) was added into the vial. Argon was used to bubble the solution for over 40 min, and the vial was closed. The polymerization was carried out at 45 °C in an oil bath for 8 h. After opening the vial and stirring the solution at 0 °C for 5 min, the polymerization was quenched. Ether/acetone (5/1, v/v) was dropwise added into the reaction solution while vigorously stirring, resulting in a pink precipitate, which was collected through centrifugation. The polymeric precipitate was further fractionated and purified. The purified product was dried, producing a polymer poly[HPMA-NHBoc]-GFLGKGLFG-poly[HPMA-NHBoc] (745 mg), with a yield of 37.2%.

The above polymer poly[HPMA-NHBoc]-GFLGKGLFG-poly[HPMA-NHBoc] (750 mg) and a monomer OEGMA (10.13 g, 20.25 mmol) were incubated in a vial and protected by argon. 45 mL solution of methanol and water (3/1, v/v) with VA044

(7.75 mg, 24 μmol) was added. The solution was bubbled with argon before the vial was closed, and polymerization was carried out at 45 °C in an oil bath for 18 h. After polymerization, the polymer samples were purified by size-exclusion fractionation using an ÄKTA fast protein liquid chromatography (FPLC) system (GE Healthcare), and the details were included in Supporting Information. After lyophilization, the product polyOEGMA-block-poly[HPMA-NHBoc]-GFLGKGLFG-poly[HPMA-NHBoc]-block-polyOEGMA was obtained (7.3 g).

The Boc groups in the above polymer (2.0 g) were deprotected through stirring the solution of TFA/DCM (1/1, v/v, 20 mL) for over 12 h. The solution was removed and the residue was dissolved in water. The aqueous solution was subjected to dialysis in water and lyophilization. The collected product was dissolved in NH_4OAc buffer (10 mL, 0.1 M, pH 5.7) and 400 mg doxorubicin hydrochloride (DOX·HCl) was added. The solution was stirred in the dark for 18 h at 25 °C. The red reaction solution was dialyzed with water through a membrane with a MW cut-off of 3.5 kDa. After lyophilization, the final product polyOEGMA-block-poly[HPMA-DOX]-GFLGKGLFG-poly[HPMA-DOX]-block-polyOEGMA (diblock polymer-DOX, 2.02 g) was obtained, and the DOX content was 6.91% (w/w) by UV-vis spectrophotometry analysis.

2.4. Preparation of CLM

DOX/NFX co-loaded micelles (CLM) and DOX-loaded micelles (DLM) were prepared in a similar manner as the thin-film hydration method. To prepare CLM, amphiphilic and block polymer polyOEGMA-block-poly[HPMA-DOX] -GFLGKGLFG-poly[HPMA-DOX]-block-polyOEGMA and NFX (5:1, molar ratio) were accurately weighed, dissolved in methanol and chloroform, and sonicated for 30 min. The mixed solvent was evaporated at 40 ℃ under vacuum. 0.01M phosphate

buffer saline (PBS, pH 7.4) was added dropwise to hydrate the thin-film. After stirring for several hours until the solids were well suspended, the solution was filtered through a 0.45 μm membrane filter to remove unloaded drugs and solid debris. The CLM was stored at 4 ℃ for further use. DLM was prepared in the similar manner except NFX. The concentration of both drugs in CLM was quantitatively determined by a UV-6100 spectrometer (Shanghai Mapada Instruments Co., Ltd., China) through their corresponding maximum absorption. The calibration curve for DOX was Y = 0.0108X - 0.007343 (R^2 = 0.9996), and the linear correlation was within the concentration range of 10 - 80 μg/mL (Figure S9a); the calibration curve for NFX was Y = 0.0771X + 0.01157 (R^2 = 0.9997), and the correlation was within the concentration range of 1.376 - 16.512 μg/mL (Figure S9b). The encapsulation efficacy, E_E, and drug loading, D_L, were calculated as the following equations:

$$E_E\ (\%) = \frac{W_L}{W_0} \times 100\% \text{ and } D_L\ (\%) = \frac{W_L}{W_0 + W_M} \times 100\%$$

where W_L was the weight of the loaded drug, W_0 the initial drug weight and W_M the weight of the micelle polymer.

2.5. Micelle size, zeta-potentials and morphology characterization

The micelle size and zeta-potential were measured with a dynamic light scattering (DLS) Zeta-sizer (Malvern Instruments, Malvern, UK). The morphology of DLM and CLM was observed under a transmission electronic microscope (TEM). Samples were stained with phosphotungstic acid solution (0.2%, w/v). To investigate the stability of DLM and CLM, the particle size of the micelles was measured by DLS, and the UV-vis was used to determine the content of DOX and NFX in the micelles.

2.6. Determination of critical micelle concentration (CMC)

The CMC of DLM was estimated through a fluorescence spectroscopy with pyrene as a probe. The pyrene solutions in acetone were added to a brown bottle, evaporating

acetone in a fume hood. 1 mL of DLM solution at different concentrations ranging from 0.001 μg/mL to 1.0 mg/mL was added to each bottle, and the final pyrene concentration was 5×10^{-6} mol/L. The solution was stirred for 24 h at room temperature in the dark. The emission spectra of pyrene were monitored by a fluorescence spectroscope with an excitation wavelength of 334 nm. The intensity ratios of I_{373}/I_{384} were plotted as a function of the logarithm of the DLM concentration.

2.7. In vitro release profiles

The release profiles of DOX and NFX from CLM were determined by using a dialysis method. The product release from the micelles was investigated in PBS (pH 7.4, pH 5.4) with or without papain. The samples were transferred into a dialysis bag (MWCO = 3500 Da), and placed them in four different media (pH = 7.4 without papain, pH = 5.4 without papain, pH = 7.4 with 2 μM papain or pH = 5.4 with 2 μM papain) at 37.0 ℃ in a shaking bed at 100 rpm. A small volume was withdrawn from different media at a predetermined time. The amount of released DOX and NFX was determined using UV at a wavelength of 488 nm and 379 nm, respectively.

2.8. Cell viability assay

The cell viability was assessed by the Cell Counting Kit (CCK-8) assay. In brief, the 4T1 cells at the exponentially growing phase were seeded to 96-well plates at 5×10^{3} /well and cultured overnight. These cells were treated with DOX, NFX, DLM, and CLM at different concentrations. After treatment for 24 h, 100 μL of fresh medium containing 10 μL of CCK-8 was added to the wells, and the plates were incubated for an additional 2 h in the dark. Finally, the absorbance was measured at 450 nm using a microplate reader.

2.9. Wound-healing migration assay

4T1 cells were seeded to 12-well plates at 5×10^5 /mL and cultured for 24 h. When cells grew to 80% confluence, the cell monolayer was scraped by sterile 200 μL pipette tips, and washed with cold PBS three times. Fresh medium containing drugs was added. After 24 h incubation, cells were observed and counted under an inverted fluorescence microscope.

2.10. Transwell migration and invasion assay

The anti-metastatic efficacy of DLM in vitro was measured in 4T1 cells by cell migration and invasion assays in an insert Transwell device. In brief, for the migration assay, 1×10^5 4T1 cells in 100 μL serum-free medium were added in the upper chamber, and 600 μL of medium containing 10% FBS was added in 24-well plates. For the invasion assay, the upper chamber was coated with diluted Matrigel by serum-free medium (1:5, 100 μL/well, DLC Biosciences), then 100 μL serum-free medium containing 1×10^5 4T1 cells was added in the upper chamber, and the lower chamber was filled with 600 μL medium with 10 % FBS. NFX, DOX, DLM or CLM was added in both chambers, and incubated for 24 h. The migrated or invaded cells were fixed with methanol and stained with 0.1% crystal violet, and the cells were photographed and counted under a light microscope.

2.11. Ex vivo biodistribution

The 4T1 cells were used for establishment of orthotropic breast cancer models by injecting 4T1 cells (5×10^5 in 100 μL) into the right mammary fat pad of the female BALB/c mice. About 2 weeks after tumor implantation, mice bearing an orthotropic model of breast cancer metastasis to lungs were intravenously injected with PBS and DLM (100 μL each mouse). After injection, mice were sacrificed at 6, 12, 36, and 48 h. The tumors and organs (hearts, livers, spleens, lungs, and kidneys) were collected and then excised to evaluate the drug distribution in tissues.

2.12. In vivo anti-cancer and anti-metastasis efficacy

Two murine models, orthotropic and lung metastasis breast cancer models, were established. The orthotropic model was constructed by injecting 5×10^5 4T1 cells into the right mammary fat pad of the female BALB/c mice. When the tumors approximately reached 150 - 200 mm^3 (1-2 weeks after implantation), mice were randomly divided into five groups with 6 mice in each group. The groups were PBS, free DOX (3 mg/kg), free NFX (5 mg/kg, intraperitoneal injection), DLM (equivalent to DOX 3 mg/kg), and CLM (equivalent to DOX 3 mg/kg, NFX 5 mg/kg). The mice were injected with 100 μL solution through tail vein (except NFX group via i.p.) every four days for 5 times in total. All mice were sacrificed on day 21. During the treatment, the tumor volume (length × $width^2$ × 0.5) and body weight were measured every 2 days [26]. The lung metastasis model was established by injecting 2×10^5 4T1 cells through tail vein of BALB/c mice. Five groups (n = 6) same as the groups for the orthotropic model were selected. 100 μL of samples was injected through tail vein (except NFX group via i.p.) on day 2 and day 6. All mice were sacrificed on day 10 due to the fatal nature of this model.

2.13. Histological Studies

Tumors and major organs such as heart, livers, spleens, lungs and kidney from both models were excised and fixed for slicing. The sections were stained using hematoxylin and eosin (H&E) for histopathological evaluation. One part of the paraffin tumor sections was stained with Ki-67, CD-31, MMP-2 and MMP-9 antibodies. The other part of the paraffin tumor section was stained for TUNEL. The lung sections were stained with Gr-1/CD11b antibodies to examine the myeloid-derived suppressor cells infiltration.

2.14. Statistical analysis

All the experiments were repeated at least three times. Data were expressed as mean ± standard deviation (SD). Results were analyzed by two-tailed Student's t-test for two groups and one-way ANOVA for multiple groups. *$p < 0.05$, **$p < 0.01$ and ***$p < 0.001$ were considered to be statistically significant.

3. Results and Discussion

3.1. Synthesis and Characterizations of prodrug and its micelles

The polyacrylamide-based polymers, including HPMA and OEGMA copolymers, have been studies as anticancer drug delivery systems [27]. PolyOEGMA and polyHPMA copolymers prepared via polymerization of HPMA and OEGMA have good biosafety and water-solubility, flexible chemistry for drug conjugating and modifications [28]. Compared to polyHPMA, polyOEGMA has similar properties as PEG, and its drug conjugate-based nanoparticles have higher stability and a long blood circulation [29, 30], which may be due to its flexible side-chains. Additionally, molecular weights (MWs) of polymers can be optimized for enhancing their EPR effect, and those polymers with larger MWs (but below 300 kDa) have been demonstrated to contribute to great accumulation in the tumor tissue [31, 32]. However, these polymeric carriers and their degraded products should be cleared via kidney, and the MWs are generally controlled below 50 kDa [33]. To achieve high accumulation and low toxicity, biodegradable polymers are prepared. Biodegradable linkers, such as GFLG peptide, have been introduced into the backbone of polyacrylamide-based polymers and the resulting dimers have also demonstrated their excellent anticancer efficacy [34, 35]. Herein, the monomers for polyOEGMA were

first prepared, purified and characterized (Figure S1-S6), and CTA-GFLGKGLFG-CTA was employed as a chain transfer agent (CTA) for RAFT polymerization, as PDI and molecular structures can be well controlled via RAFT polymerization. To prepare an amphiphilic and block polymer, the monomer HPMA and MA-NHNHBoc were polymerized, and the resulting polymer poly[HPMA-NHBoc]-GFLGKGLFG-poly[HPMA-NHBoc] was employed as macroCTA for further polymerization of the hydrophilic monomer OEGMA (Figure 1). The biodegradable GFLGKGLFG linker was introduced to the backbone, which was confirmed via amino acid analysis (Table S1). The product was purified and no monomers were observed. The Boc groups on the polymer polyOEGMA-block-poly[HPMA-NHBoc]-GFLGKGLFG-poly[HPMA-NHBoc]-block-polyOEGMA were removed in TFA solvents, and ^{1}H NMR spectra of product without Boc groups was shown in Figure 2a and Figure S8. The peaks appeared at 7.00-7.50 ppm were assigned to the aromatic ring protons from the Phe moiety in GFLG and amide-amide hydrogen. The small molecular drug DOX was covalently conjugated to the polymeric carrier via an acid–labile hydrazone bond, which was confirmed via UV–vis spectrophotometry analysis. Additionally, some characteristic peaks of DOX-moieties were observed in the ^{1}H NMR spectra (Figure 2b), which were labeled with arrows. The MW and PDI of the amphiphilic and block polymer polyOEGMA-block-poly[HPMA-DOX]-GFLGKGLFG-poly[HPMA-DOX]-block-po

lyOEGMA (polymeric prodrug) were measured using SEC analysis. The MW of the final product was 92 kDa with a PDI of 1.12 (Figure 2c).

The DOX-conjugated polymeric prodrug self-assembled into micelles (DLM) in PBS (pH = 7.4) above the critical micelle concentration (CMC) of 0.025 mg/mL. Such a low CMC value enabled the micelles to be a stable systemic drug delivery system (DDS) even when diluting in the blood stream during circulation (Figure S10). NFX was non-covalently wrapped into the prodrug materials via thin-film hydration to form both drug co-loaded micelles (CLM) via self-assembly. The driving forces for the self-assembly process may be attributed to the minimization of the interfacial energy governed by the interaction balance between hydrophilic HPMA/PEOGMA moieties and hydrophobic DOX/NFX and the cathepsin B sensitive peptide GFLG in the micelle core. The interactions between DOX and NFX could provide forces such as the π-π stacking, dipole interactions and H-bonding. Additionally, GFLG is a tetra-peptide with sequence of Gly–Phe–Leu–Gly which has a certain degree of hydrophobicity.

The characteristic absorption peaks of DOX and NFX were at 488 nm and 379 nm (Figure 3a), respectively indicating that the covalently and non-covalently loaded drugs co-existed in micelles. Dynamic light scattering (DLS) results showed that the average size of DLM and CLM was 80.60 ± 0.51 nm and 131.33 ± 6.0 nm, and PDI of 0.25 and 0.24, respectively (Figure 3b). Both DLM and CLM displayed a spherical shape under a TEM and they had a diameter of 44.30 ± 3.70 nm and 67.30 ± 7.00 nm, respectively (Figure 3c and 3d). The reduced diameter in TEM images was possibly due to dehydration of micelles during pre-treatment for TEM. DOX/NFX and GFLG peptide were assembled into the hydrophobic core, and the hydrophilic layer of HPMA and POEGMA was stretched from inside out.

The zeta potential value of DLM and CLM was - 4.37 ± 0.99 mV and - 5.62 ± 0.92 mV, and the negatively charged surface allowed not being recognized by macrophages in the endothelial reticulum system and extending the blood circulation time (Table S2). The encapsulated rate and the loading capacity of NFX in CLM was optimized as 65.4% and 11.5%, respectively (Table S3). CLM was formed by self-assembly or aggregation of the hydrophobic core which was composed of GFLG and DOX/NFX π-π stacking. The drive force for the self-assembly was to minimize the interfacial energy, which resulted from the amphiphilic property of the polymer. The DOX moieties were constituted with amino groups, hydroxyl groups and aromatic groups. Interactions among these groups may generate other driving forces, such as H-bonding and π-π stacking. NFX was encapsulated into the inner hydrophobic core because the interaction between NFX and DOX-based moieties facilitated the NFX loading when the polymeric prodrug was utilized as micelles.

As presented in Figure S11, the micelles were stable at room temperature without significant size variation. The results indicated that the micelles had excellent physical stability which could be attributed to a low CMC of the polymeric prodrug. Due to pH and enzymatic sensitivity of the structural material, the release profile of CLM was investigated by dialysis against PBS (pH 7.4 and 5.4) at 37 °C in the presence/absence of papain which has a similar activity as lysosomal cathepsin B. In two acidic media, complete release of DOX was achieved within 36 h, on the contrary, less than 10% of DOX was released after 48 h under a neutral pH (Figure 3e). The releasing rate was accelerated in the presence of the enzyme. Moreover, non-covalently loaded NFX was released faster than DOX in the medium at pH 5.4 without papain, which indicated that breakage of the hydrazone bond could destroy the micelle structure (Figure 3f). The nitrogen on the carbon–nitrogen double bond of hydrazone could attach to an

amine or imine group which could be quickly hydrolyzed in acidic conditions to form esters [36, 37]. DOX as the micelle core component was liberated through this process and the π-π stacked NFX was therefore released. Following enzymatic digestion of the GFLG linker, the inner hydrophobicity in the micelles was further weakened and the macromolecules were degraded into smaller fragments. This accelerated the process of disintegrating the micelle structure, resulting in complete drug release.

Furthermore, in order to confirm the liberating drugs maintaining their inherent structures in their free form, the CLM releasing medium (pH 5.4 with papain) was sampled at 24 h and analyzed by liquid chromatography-mass spectrometry (LC-MS). As shown in Figure 3g and 3h, ESI-MS was utilized to analyze DOX and NFX individually and abundant peaks of 544.30 $[M-H]^-$ and 276.00 $[M+H]^+$ were detected, corresponding to DOX and NFX, respectively. This suggested the detaching DOX molecules from the polymer backbone was the same as free DOX, and they should have the same pharmaceutical efficacy and side effects as free DOX. The degradation characteristics of the polymeric prodrug were revealed via the SEC study. As shown in Figure 2, CLM was degraded to low MWs segments in the presence of Cathepsin B, and the low MW was about 39 kDa (Figure 2d) which was less than the renal threshold, 50 kDa. That was due to the cleavage of the GFLGKGLFG linker in the backbone of the polymeric prodrug. These results indicated that CLM was rapidly degraded to low MWs segments at tumor sits/cells after releasing DOX and NFX, demonstrating its great potential as an efficient and safe anticancer nanoscale agent.

3.2. In vitro cytotoxicity and anti-metastatic efficacy

The cytotoxicity evaluation was carried out by CCK-8 assays of 4T1 cells. The IC_{50} of CLM, DLM, free NFX and free DOX were 8.93, 10.88, 1.74 and 0.48 μg/mL

(Figure S12). Both free drugs showed better anti-cancer efficacy than CLM. This might be caused by the prolonged drug release of CLM via endocytosis process which was much slower than passive diffusion of free drugs. However, hydrophobic drugs in the positive control groups were dissolved in membrane destructive solvent, DMSO, which restricted these drugs in the in vivo application. The prodrug micelles could be an excellent carrier for simultaneously delivering different combinational recipes.

Migration and invasion are key steps in the development of breast cancer metastasis. Inhibition of metastasis is a crucial approach against cancer. Wound healing assays and Transwell assays were used to evaluate inhibition of migration and invasion 4TI cells. CLM displayed an outstanding effect against 4T1 cell migration with a healing rate of 12.3%, while the control group completely healed the cell wound after 24 h of incubation (Figure 4a and Figure S13). According to the Transwell migration and Matrigel invasion assays, CLM clearly inhibited metastasis of 4T1 cells in a dose-dependent manner (Figure 4b and 4d). 4T1 cells exhibited a significant reduction in migration and invasion in the presence of NFX (Figure 4c and 4e). Therefore, the combination therapy by DOX and NFX showed strong inhibition of tumor cell proliferation and prevention of metastasis.

3.3. Ex vivo biodistribution

The time-dependent biodistribution was measured to predict accumulation and destination of CLM. The murine orthotropic breast cancer model was established by injecting 4T1 cells into the right mammary fat pad of female BALB/c mice. CLM was intravenously injected and the accumulated amount of DOX in tumor reached the maximum at 36 h by counting its average fluorescence intensity (Figure 5a and 5b). On the contrary, an equivalent amount of free DOX rarely resided in tumor and it was eliminated through liver (Figure S14). The results indicated that CLM could target

tumor via the size-dependent EPR effect and DOX in CLM could retain in tumor for more than 48 h. The fluorescence was distributed in the core of tumor, which suggested preferable deep penetration of CLM for anti-cancer therapy. One may notice that a portion of the drug released from CLM was transported to the lung region and fluorescence signals remained strong for 48 h. It was speculated that the DDS could not only target solid tumor but also retain inside pulmonary metastasis. Moreover, the DDS stayed in the circulation system without uptake by reticuloendothelial cells in the first 6 h, which assisted in drug accumulation at the target site. During the experimental period, the drug was mainly metabolized through liver and kidney which will be improved in the further study by modifying micelle surfaces with 'invisible' groups.

3.4. In vivo anticancer and anti-metastasis efficacy

The anti-cancer and anti-metastasis efficacy of CLM against breast cancer was evaluated on two murine models: orthotropic and lung metastasis breast cancer model. The orthotropic model was established by injecting 4T1 cells into the right mammary fat pad to form a solid tumor and distinct metastasis involved lung, liver and regional lymph nodes. CLM significantly suppressed growth of the tumor in mammary via i.v. injection every 4 days for 5 times (Figure 5c). The tumor growth inhibition (TGI) rate of CLM was 56.92%, which was significantly higher than 26.99% of DLM on the 21st day (Figure 5d). Compared to a low survival rate of other treatments, 100% survival rate in the CLM group was observed on day 21 post-treatment (Figure S16a). Furthermore, lung is one of main metastatic target organs by malignant breast cancer and the number of lung nodules was counted to quantify the level of metastasis. The least number of lung nodules was found in the CLM group, around 4 times less than the control (Figure 5e).

In order to further confirm the anti-metastatic effect of CLM, the lung metastasis model was established by injecting 4T1 cells through tail vein of mice. The mice were sacrificed on day 10 and lungs were harvested to quantify the nodules. CLM was i.v. injected on day 2 and day 6, resulting in effective inhibition of the malignant tumor cells seeding in the pulmonary region (Figure 6a). The pulmonary organs from scarified mice displayed healthy appearance when treating with CLM. (Figure 6c) On the contrary, the control group exhibited a high degree of metastasis and typically more than 30 nodules were found in lung on the 10^{th} day. Moreover, treatment by CLM lead to a prolonged survival rate for up to 10 days. (Figure S16b) Meanwhile, insignificant shift in the body weight was observed during the treatment. (Figure 6b) NFX for in vivo anti-metastasis studies was often administered by intraperitoneal (i.p.) injection at 10-50 mg/kg in mice breast cancer models and 0.1% DMSO was used as a vehicle. This micelle system allowed NFX to be administered by i.v., which improved the druggability of NFX. More importantly, NFX in CLM administrated at 5 mg/kg had a similar anti-metastasis efficacy as the 50 mg/kg group in the reported research [30]. Due to high complexity of the metastasis processes in breast cancer development, it is crucial to develop a smart system that can automatically track the target organ and deliver the drug. The stimuli-sensitive prodrug micelles, CLM, not only assisted in accumulating both drugs at the tumor site by the EPR effect, but also travelled to organs due to unpredictable metastasis, especially in lung. The controlled release property of CLM could alleviate the toxicity of both therapeutic agents to health cells, thus could enhance the drug tolerance.

3.5. Histological studies

In order to further identify pathologic changes, apoptosis, proliferation, invasion and metastasis after the treatments, the excised tumors and main organs from each

group of both animal models were stained by H&E, TUNEL, IHC and IF. The H&E staining images of major organs indicated that no clear pathologic changes were detected in the CLM group. (Figure S15) Comparing with the severe cardiotoxicity in the free DOX group, CLM improved biosafety of DOX at the same DOX dose. The TUNEL staining was used to identify apoptotic cells by detecting the breakage of nuclear DNA and the positive apoptotic nuclei displayed a green color. As shown in Figure S17, a strong fluorescence intensity in the fat pad was found in the CLM group, indicating a large population of apoptotic tumor cells. TUNEL-positive cells were further counted and the percentage of TUNEL-positive cells in the CLM group was about 67.7%. These results suggested that CLM had very potent anti-cancer effects.

Ki67 is a nuclear antigen associated with tumor cell proliferation and its expression is closely related to the cell cycle. The positively Ki67 staining cells with a light yellowish color have a strong proliferation ability. It can be seen from Figure 7a that the number of Ki67-positive cells in the orthotropic tumor tissue after CLM treatment were significantly reduced. Similar results were found in the pulmonary staining section of the lung metastasis breast cancer model, demonstrating CLM could inhibit tumor cell proliferation. The blood vessels density in tumor is relevant to metastasis. CD31 is a transmembrane glycoprotein expressed especially at the junction of vascular endothelial cells in tumor tissues and the amount of CD31 is positively correlated with the tumor vascular density. The results indicated that CLM could significantly inhibiting angiogenesis in both models, thus preventing metastasis of cancer tissue cells. (Figure 7a) Furthermore, CLM could block the matrix metalloproteinase (MMP) pathway by suppressing the expression of two matrix metalloproteinase associated with metastasis.

3.6. Infiltration of MDSCs on lungs

Dual-immunofluorescence staining of Gr-1 and CD11b was performed on frozen sections of the lungs to examine infiltration of myeloid-derived suppressor cells (MDSCs) which are immunosuppressive cells accumulated in highly metastatic carcinoma [38]. The results showed that a large number of Gr-1+CD11b+ cells were seen in the PBS group, in contrast, positive cells were rarely found in the CLM group in both models. These results indicated that CLM effectively reduced the infiltration of MDSCs into the lungs and inhibited the distant metastasis of tumor cells, and lung metastasis of breast cancer (Figure 7b). The histological study demonstrated the underlying anti-metastasis activity of CLM. It could be synergistic action of suppressing the expression of MMP-2 and MMP-9 associated with invasion and metastasis, inhibiting angiogenesis generation and MDSCs infiltration.

4. Conclusions

A pH and cathepsin B dual sensitive polymeric prodrug conjugated with DOX and loaded with NFX in the form of micelles was prepared to precisely deliver both drugs to treat breast cancer and lung metastasis. The drug-loaded micelles accumulated at the tumor site after i.v. administration and controlled release of their cargos was realized by cleaving hydrazone and GFLG bonds via stimuli-responsiveness inside the tumor microenvironment. CLM enhanced the anti-tumor efficacy of free drugs and exerted great anti-metastatic effect in both orthotropic and lung metastasis breast cancer models. A large population of apoptotic cells were induced, and the metastasis-relevant MMP pathway and MDSCs infiltration were inhibited for pulmonary metastasis after CLM treatment. Furthermore, CLM showed excellent biocompatibility with main organs and reduced the cardiotoxicity of DOX. Therefore, CLM may hold great potential against primary breast cancer and pulmonary metastasis.

Competing Interest

We also declare that there aren't competing financial interests in relation to the work described.

Authors' contributions

L.L. and K.L. designed the study; F.X. and H.P. acquired, analyzed and interpreted the data; and L.L., F.X., H.P., Z.G. and K.L. drafted the manuscript and L.L., F.X., H.P., Q.G., H. Z., G.B., Z.G. and K.L. critically revised the manuscript. All authors approved the final version of the manuscript.

Declarations of Competing Interest

None.

Acknowledgments

This research was financially supported by the National Natural Science Foundation of China (51873120, 51873127, 81621003), National Science and Technology Major Project of China (2017ZX09304023), Fundamental Research Funds for the Central Universities (XDJK2019TY002), National key research and development program of China (2017YFD0501404). We are grateful to Sisi Wu, Xuemei Chen, Zhiqian Li and Yinchan Wang (Core Facility of West China Hospital, Sichuan University) for their help in cell data analysis and polymer synthesis.

Appendix A. Supplementary data

Supplementary data to this article can be found online.

References

[1] M. Yousefi, R. Nosrati, A. Salmaninejad, S. Dehghani, A. Shahryari, A. Saberi, Organ-specific metastasis of breast cancer: molecular and cellular mechanisms underlying lung metastasis, Cell. Oncol. 41(2018) 123-140.

[2] L. T. Jin, B. C. Han, E. Siegel, Y. K. Cui, A. Giuliano, X. J. Cui, Breast cancer lung metastasis: Molecular biology and therapeutic implications, Cancer Biol. Ther. 19 (2018) 858-868.

[3] S. Sponholz,M. Schirren, N. Kudelin, E. Knochlein, J. Schirren, Results of Pulmonary Resection Other Epithelial Malignancies, Thorac. Surg. Clin. 26 (2016) 99-108.

[4] C. Liang,L.G. Xu, G. S. Song, Z. Liu, Emerging nanomedicine approaches fighting tumor metastasis: animal models, metastasis-targeted drug delivery, phototherapy, and immunotherapy, Chem. Soc. Rev. 45 (2016) 6250-6269.

[5] J. J. Shi, P. W. Kantoff, R. Wooster, O. C. Farokhzad, Cancer nanomedicine: progress, challenges and opportunities, Nat. Rev. Cancer 17 (2017) 20-37.

[6] S. Mura, J. Nicolas, P. Couvreur, Stimuli-responsive nanocarriers for drug delivery. Nat. Mater. 12 (2013) 991-1003.

[7] S. Dragojevic, J. S. Ryu, D. Raucher, Polymer-based prodrugs: improving tumor targeting and the solubility of small molecule drugs in cancer therapy, Molecules 20 (2015) 21750-21769.

[8] S. T. Gao, G. S.Tang, D. W. Hua, R. H. Xiong, J. Q. Han, S. H. Jiang, Q. L. Zhang, C. B. Huang, Stimuli-responsive bio-based polymeric systems and their applications, J. Mater. Chem. B 7 (2019) 709-729.

[9] D. Rosenblum, N. Joshi, W. Tao, J. M. Karp, D. Peer, Progress and challenges towards targeted delivery of cancer therapeutics, Nat. Commun. 9 (2018) 1410-1422.

[10] L. Luo, Q. Zhang, Y. Luo, Z. He, X. Tian, G. Battaglia, Thermosensitive nanocomposite gel for intra-tumoral two-photon photodynamic therapy, J. Control. Release 298 (2019) 99-109.

[11] C. Luo, J. Sun, B. J. Sun, Z. G. He, Prodrug-based nanoparticulate drug delivery strategies for cancer therapy, Trends Pharmacol. Sci. 35 (2014) 12-22.

[12] H. Cabral, K. Miyata, K. Osada, K. Kataoka, Block copolymer micelles in nanomedicine applications. Chem. Rev. 118 (2018) 6844-6892.

[13] F. Zhang, Q. Ni, O. Jacobson, S. Cheng, A. Liao, Z. Wang, Z. He, G. Yu, J. Song, Y. Ma, G.Niu, L. Zhang, G. Zhu, X. Chen, Polymeric nanoparticles with a Glutathione-sensitive heterodimeric multifunctional prodrug for In vivo drug monitoring and synergistic cancer therapy, Angew. Chem. Int. Edit. 57 (2018) 7066-7070.

[14] C. Wang, L.Liu, H. Cao, W. Zhang, Intracellular GSH-activatable galactoside supramolecular photosensitizers for targeted photodynamic therapy and chemotherapy, J. Control. Release 259 (2017) 135-136.

[15] G. Saravanakumar, J. Kim, W. J. Kim, Reactive-oxygen-species-responsive drug delivery systems: Promises and Challenges, Adv. Sci. 4 (2017) 1600124-1600143.

[16] N. Li, H. Cai, L. Jiang, J. Hu, A. Bains, J. Hu, Q. Gong, K. Luo, Z. Gu, Enzyme-Sensitive and Amphiphilic PEGylated Dendrimer-Paclitaxel Prodrug-Based Nanoparticles for Enhanced Stability and Anticancer Efficacy, Acs. Appl. Mater. Inter. 9 (2017) 6865-6877.

[17] H. Li, X. Yang, Z. Zhou, K. Wang, C. Li, H. Qiao, D. Oupicky, M. Sun, Near-infrared light-triggered drug release from a multiple lipid carrier complex using an all-in-one strategy, J. Control. Release 261 (2017) 126-137.

[18] S. Carregal-Romero,M. Ochs, P. Rivera-Gil, C. Ganas, A. M. Pavlov, G. B. Sukhorukov, W. J. Parak, NIR-light triggered delivery of macromolecules into the cytosol, J. Control. Release 159 (2012) 120-127.

[19] J. Liu, Y. Huang, A. Kumar, A. Tan, S. Jin, A. Mozhi, X. J. Liang, pH-sensitive nano-systems for drug delivery in cancer therapy, Biotechnol. Adv. 32 (2014) 693-710.

[20] M. L. Hou, Y. E. Gao, X. X. Shi, S. Bai, X. Q. Ma, B. S. Li, B. Xiao, P.Xue, Y. J. Kang,Z. G. Xu, Methotrexate-based amphiphilic prodrug nanoaggregates for co-administration of

multiple therapeutics and synergistic cancer therapy, Acta Biomater. 77 (2018) 228-239.

[21] W. Islam, J. Fang, T. Etrych, P. Chytil, K. Ulbrich,A.Sakoguchi, K. Kusakabe, H. Maeda, HPMA copolymer conjugate with pirarubicin: in vitro and ex vivo stability and drug release study, Int. J. Pharm. 536 (2018) 108-115.

[22] N. Li, N. Li, Q. Yi, K. Luo, C. Guo, D. Pan, Z. Gu, Amphiphilic peptide dendritic copolymer-doxorubicin nanoscale conjugate self-assembled to enzyme-responsive anti-cancer agent, Biomaterials 35 (2014) 9529-9545.

[23] S. Guo, X. Xiao, X. Wang, Q. Luo, H. Zhu, H. Zhang, H. Li, Q. Gong, K. Luo, Reductive microenvironment responsive gadolinium-based polymers as potential safe MRI contrast agents, Biomater. Sci. 7 (2019) 1919-1932.

[24] Y. Zhu, T. Ye, X. Yu, Q. Lei, F. Yang, Y. Xia, X.Song, L.Liu, H. Deng, T. Gao, C. Peng, W. Zuo, Y. Xiong, L. Zhang, N. Wang, L. Zhao, Y. Xie, L. Yu, Y.Wei, Nifuroxazide exerts potent anti-tumor and anti-metastasis activity in melanoma, Sci. Rep. 6 (2016) 20253-20266.

[25] F. Yang, M. Hu, Q. Lei, Y. Xia, Y. Zhu, X. Song, Y. Li, H. Hu, C. Liu, Y. Xiong, Z. Zuo, A. Zeng, Y. Li, L.Yu, G. Shen, D. Wang, Y. Xie, T. Ye, Y. Wei, Nifuroxazide induces apoptosis and impairs pulmonary metastasis in breast cancer model, Cell Death Dis. 6 (2015) 1701-1712.

[26] T. Takahashi, Y. Yamada, K. Kataoka, Y. Nagasaki, Preparation of a novel PEG-clay hybrid as a DDS material: Dispersion stability and sustained release profiles, J. Control. Release 107 (2005) 408-416.

[27] M.Talelli, C. J. Rijcken, C. F. van Nostrum, G. Storm, W. E. Hennink, Micelles based on HPMA copolymers. Adv. Drug. Deliv. Rev. 62 (2010) 231-239.

[28] H. Wei, J. G. Schellinger, D. S. Chu, S. H. Pun, Neuron-targeted copolymers with sheddable shielding blocks synthesized using a reducible, RAFT-ATRP double-head agent, J. Am. Chem. Soc. 134 (2012) 16554-16557.

[29] H. Wei, J. A. Pahang, S. H. Pun, Optimization of brush-like cationic copolymers for nonviral gene delivery, Biomacromolecules 14 (2013) 275-84.

[30] Y. Dai, H. Cai, Z. Duan, X. Ma, Q. Gong, K. Luo, Z. Gu, Effect of polymer side chains on drug delivery properties for cancer therapy, J. Biomed. Nanotechnol. 13 (2017) 1369-1385.

[31] R. Liu, W. Xiao, C. Hu, R. Xie, H. Gao, Theranostic size-reducible and no donor conjugated gold nanocluster fabricated hyaluronic acid nanoparticle with optimal size for combinational treatment of breast cancer and lung metastasis, J. Control. Release 278 (2018) 127-139.

[32] K. Chen, S. Liao, X. Zheng, B. Wang, Z. Duan, H. Zhang, Q. Gong, K. Luo, Multistimuli-responsive PEGylated polymeric bioconjugate-based nano-aggregate for cancer therapy, Chem. Eng. J. 2019, In Press, doi.org/10.1016/j.cej.2019.123543.

[33] T.Ishihara, M. Takahashi, M. Higaki, Y.Mizushima, T. Mizushima, Preparation and characterization of a nanoparticulate formulation composed of PEG-PLA and PLA as anti-inflammatory agents, Internat. J. Pharmaceut. 385 (2010) 170-175.

[34] L.Zhu, R. I. Mahato, Lipid and polymeric carrier-mediated nucleic acid delivery, Expert Opin. Drug Deliv. 7 (2010) 1209-1226.

[35] K. Chen, H. Cai, H. Zhang, D. Pan, Q. Gong, Z. Gu, K. Luo, Stimuli-responsive polymer-doxorubicin conjugate: Antitumor mechanism and potential as nano-prodrug. Acta

Biomater. 84 (2019) 339-355.

[36] Y. Ma, X. Fan, L. Li, pH-sensitive polymeric micelles formed by doxorubicin conjugated prodrugs for co-delivery of doxorubicin and paclitaxel, Carbohyd. Polym. 137 (2016) 19-29.

[37] Y. Yin, C. Fu, M. Li, X. Li, M. Wang, L. He, L. M. Zhang, Y. Peng, A pH-sensitive hyaluronic acid prodrug modified with lactoferrin for glioma dual-targeted treatment, Mater. Sci. Eng. C Mater. Biol. Appl. 67 (2016) 159-169.

[38] D. Escors, T. Liechtenstein, N. Perez-Janices, J. Schwarze, I. Dufait, C. Goyvaerts, A. Lanna, F. Arce, I. Blanco-Luquin, G. Kochan, D. Guerrero-Setas, K. Breckpot, Assessing T-cell responses in anticancer immunotherapy: Dendritic cells or myeloid-derived suppressor cells? Oncoimmunology 2 (2013) 26148-26157.

Figures

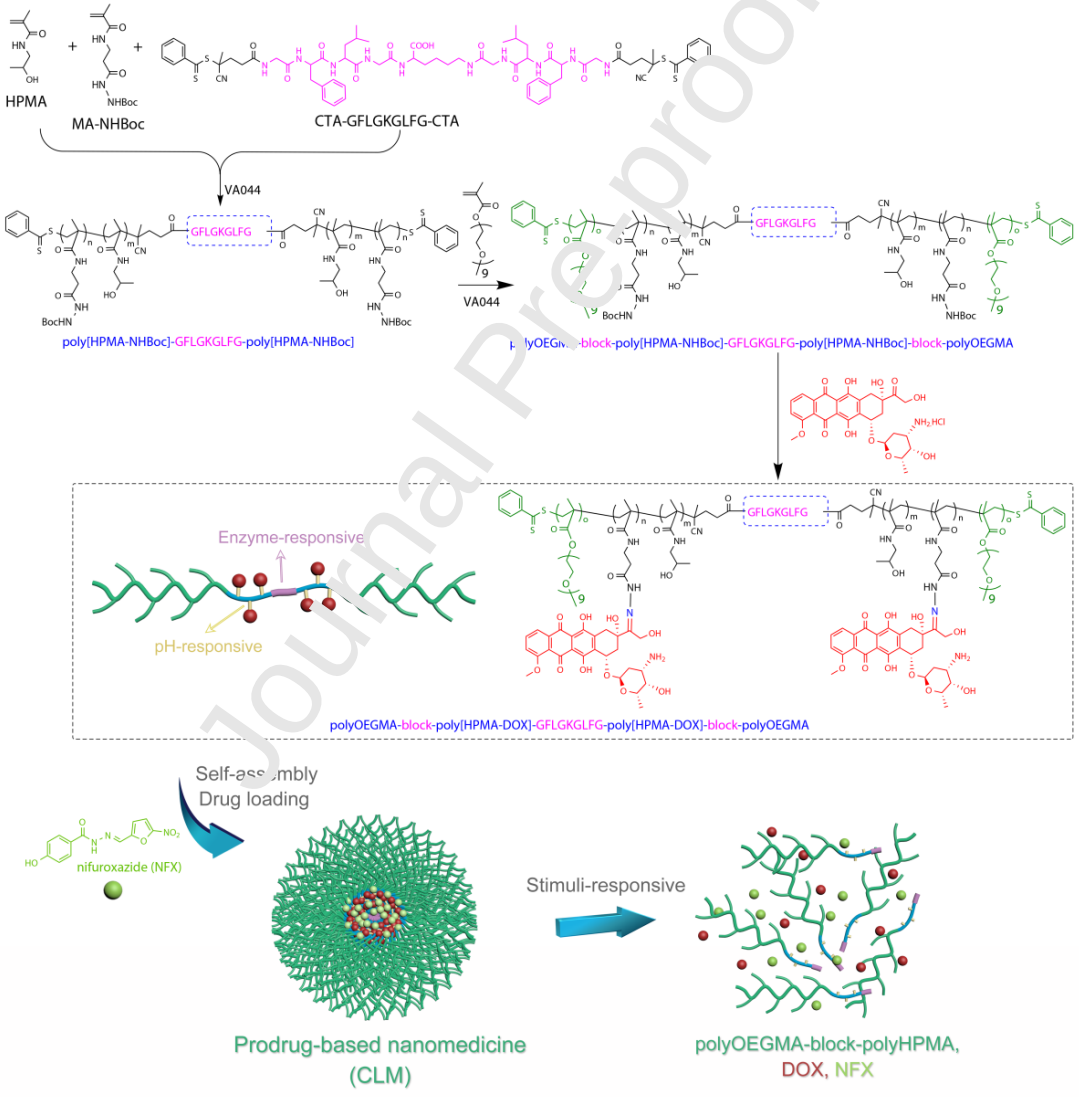

Figure 1. Preparation of block polymers; conjugation with DOX, loading with NFX, and self-assembly of micelles, and illustration of stimuli-responsive drug release and degradation.

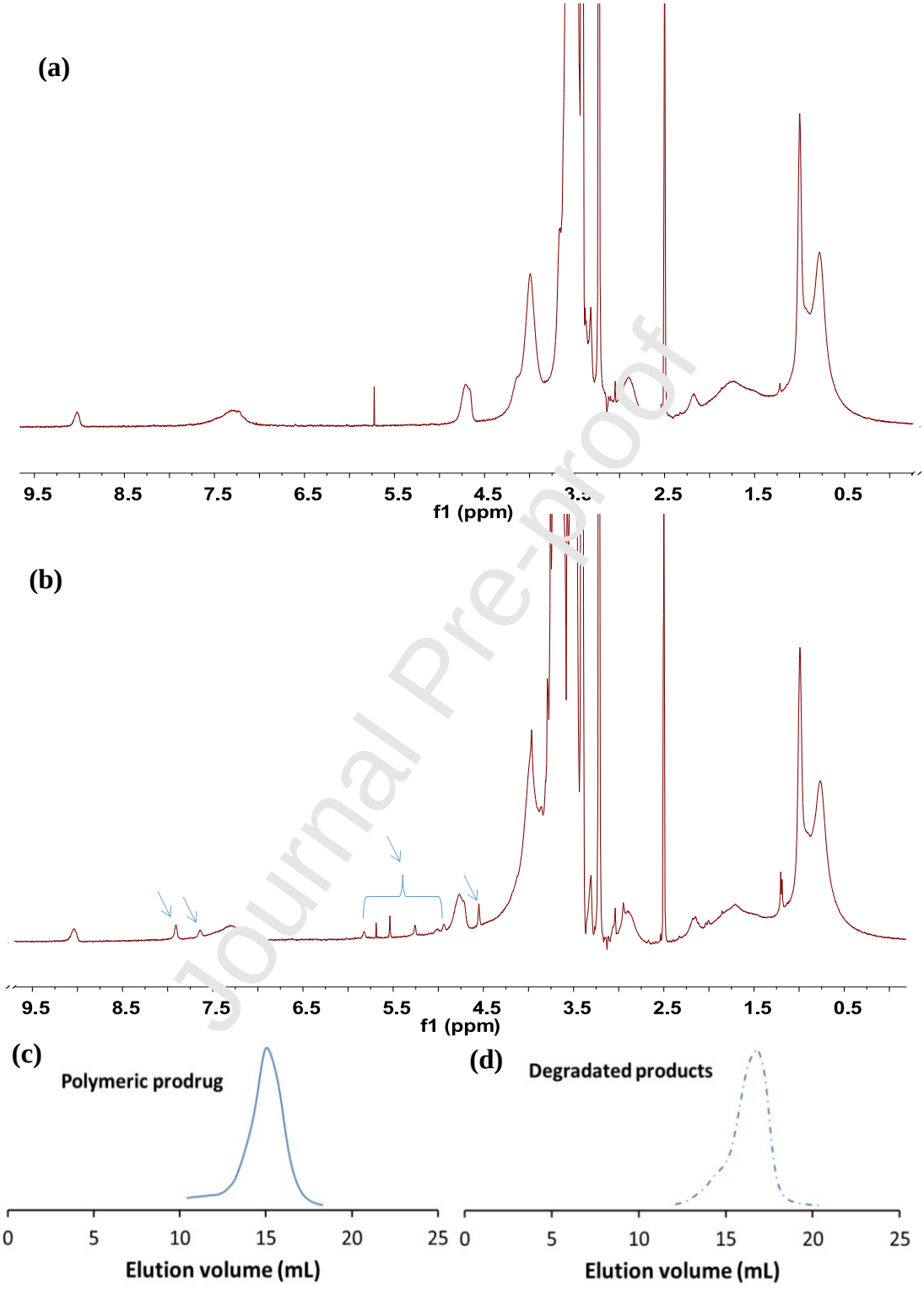

Figure 2. The ^{1}H NMR spectra of block polymer without Boc groups (a) and its DOX conjugated copolymer (polymer prodrug) (b) (recorded in d6-DMSO). Size-exclusion chromatograms of the polymeric prodrug (MW 92 kDa, PDI 1.12) (c) and its degraded products (MW 39 kDa) (d). The SEC traces were measured via an AKTA FPLC system.

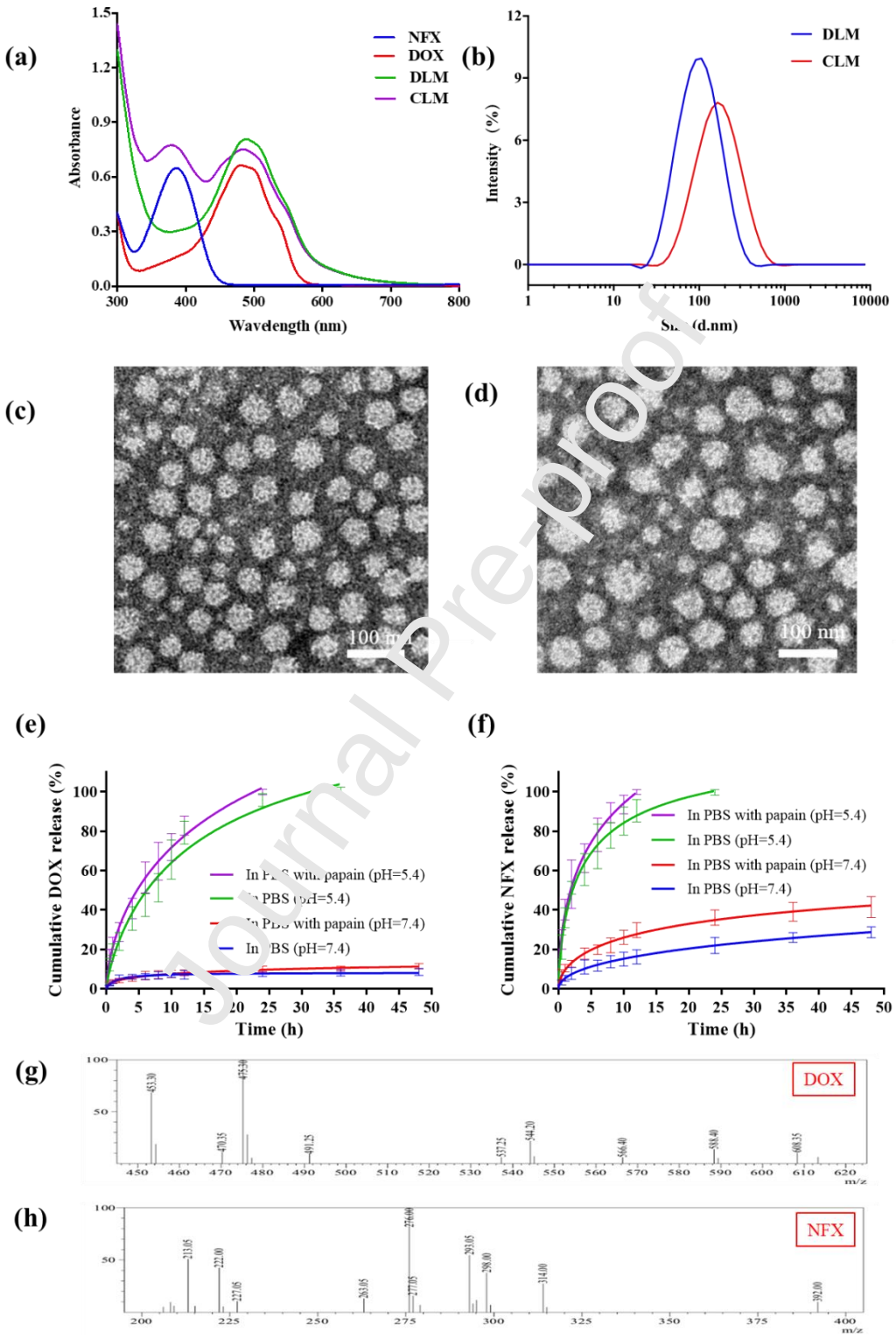

Figure 3. (a) UV-Vis spectra of free NFX, free DOX, DLM and CLM, (b) Size distribution of DLM and CLM by DLS, TEM images of (c) DLM and (d) CLM, in vitro releasing profiles of (e) DOX and (f) NFX from CLM in four different media

(n=3, error bars represent ±SD), LC-MS spectra of released (g) DOX and (h) NFX drawing from pH 5.4 media with papain at 24 hr.

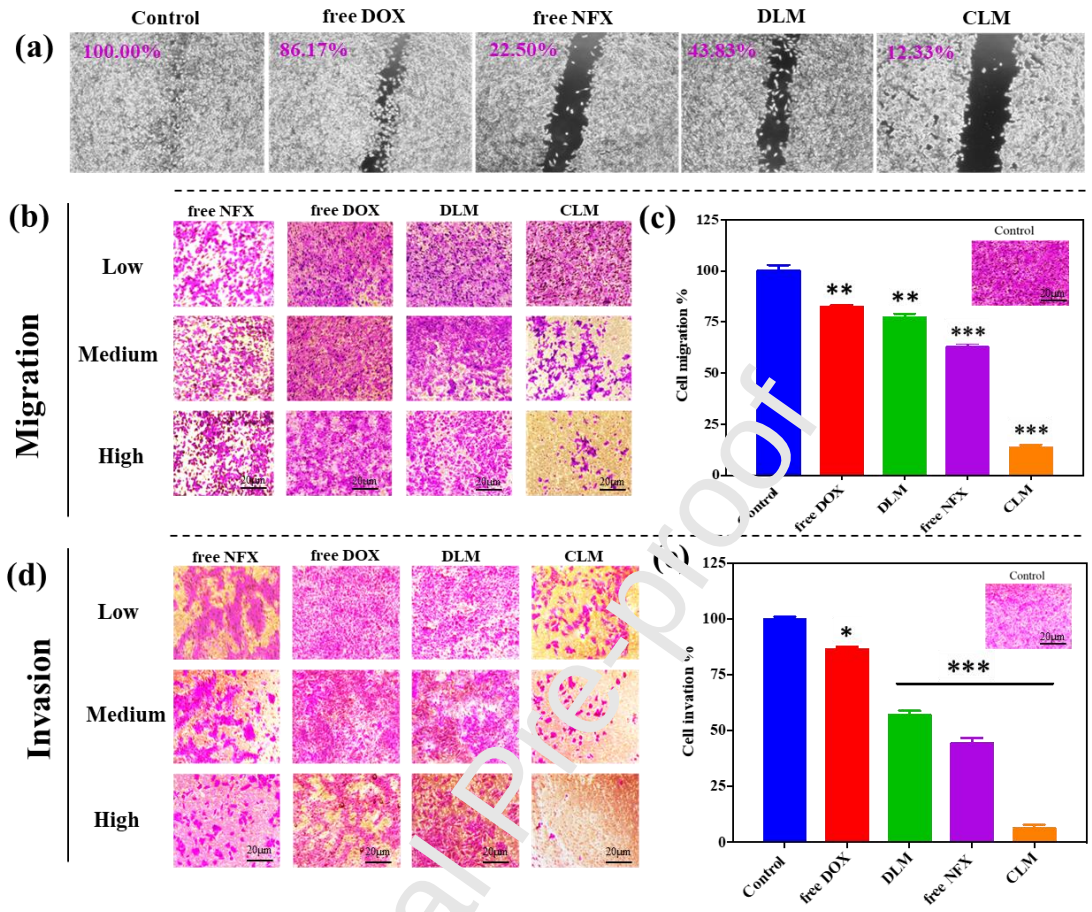

Figure 4. (a) Microscopy images of 4T1 cells wound-healing migration assay with a wound created after the cells at about 90% confluence, and the healing rates with corresponding concentrations for each group. DOX: 0.38 μg/mL and NFX: 1.38 μg/mL); (b) microscopy images and (c) quantitative analysis of Transwell migration assay. **p < 0.01 ,***p < 0.001 compared to control group, (d) microscopy images and (e) quantitative analysis of fixed cells invade through Matrigel. *p < 0.05,***p < 0.001 comparing to control group. The scale bar is 20 μm. (The corresponding concentrations for each group are: Low: DOX: 0.10 μg/mL and NFX:0.35 μg/mL, Medium: DOX: 0.19 μg/mL and NFX: 0.69 μg/mL; High: DOX: 0.38 μg/mL and NFX: 1.38 μg/mL.)

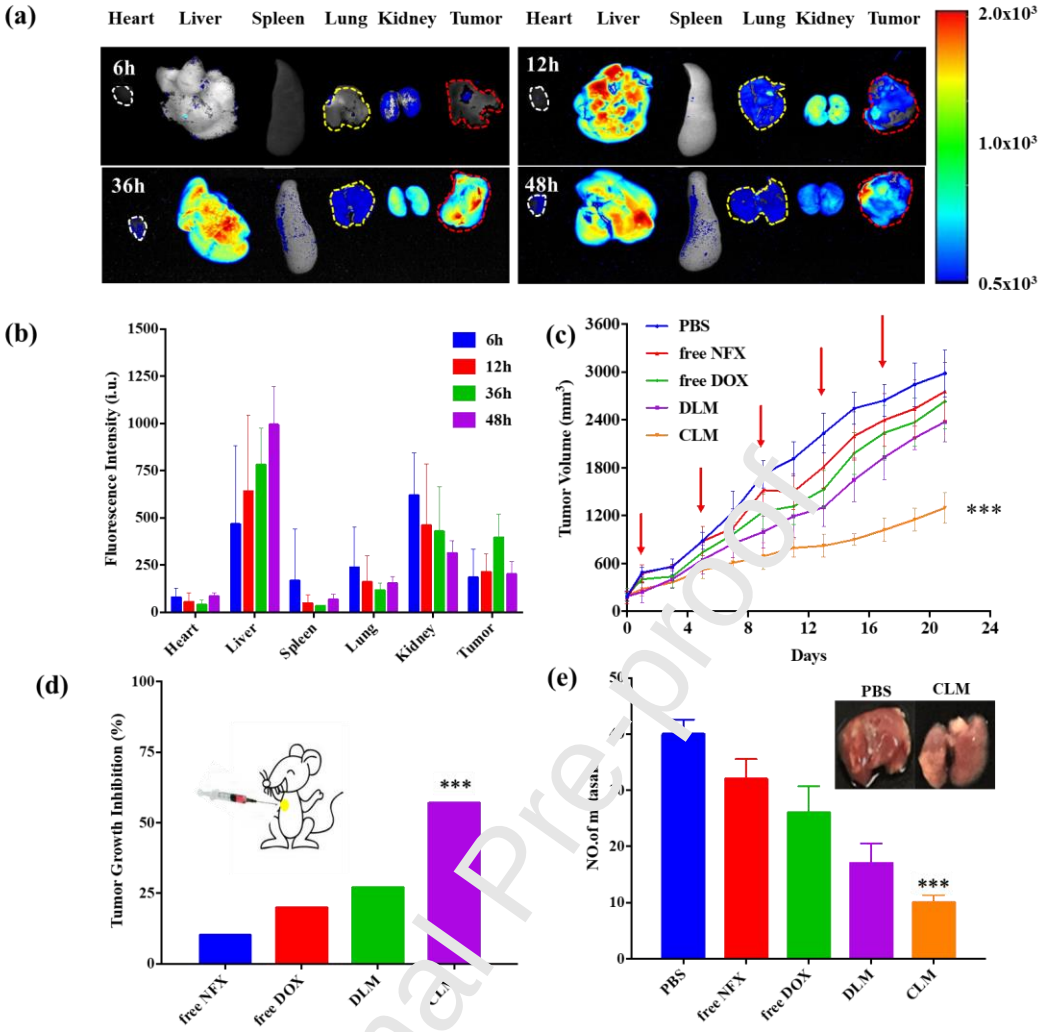

Figure 5. (a) Time dependent ex vivo distribution in the orthotropic model after i.v. injection of CLM; (b) quantitative analysis of accumulation of CLM in organs and tumor, n=3, error bars represent ±SD; in vivo anti-cancer efficacy in the orthotropic murine breast cancer model (n=6); (c) tumor growth curves, the red arrows refer to the injection time points, free NFX applied via i.p. injection; (d) tumor growth inhibition rate; (e) mean lung metastasis nodules, the inset is for excised lungs from PBS and CLM group; the agent concentration: DOX 3 mg/kg, NFX 5 mg/kg.

***p < 0.001 comparing to PBS group, error bars represent ±SD.

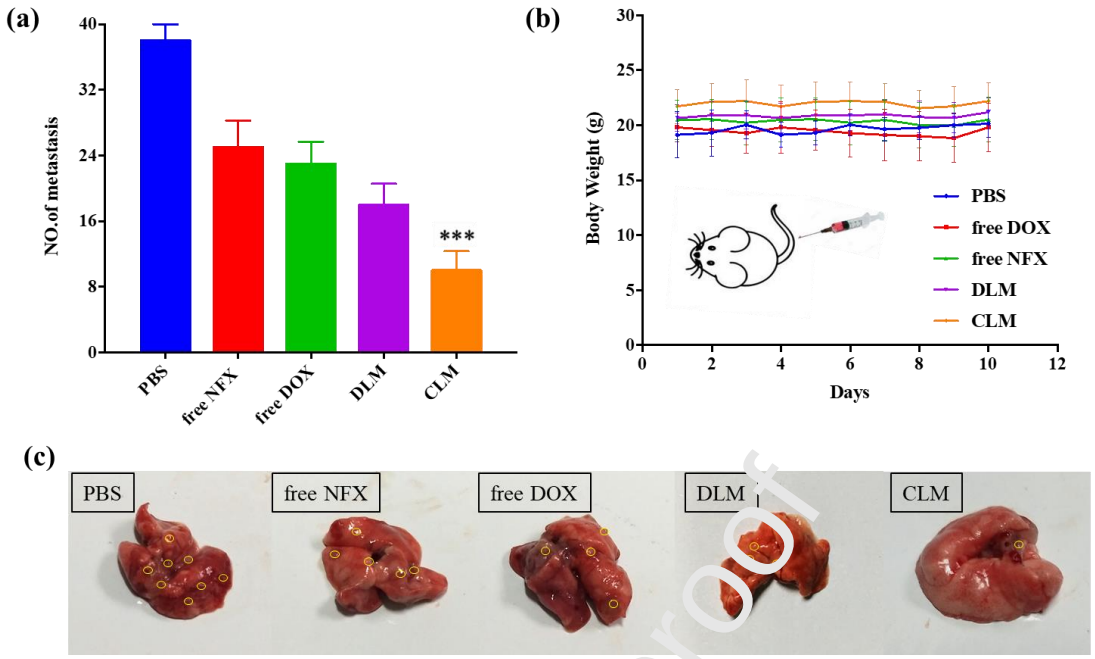

Figure 6. in vivo anti-cancer efficacy evaluated for a lung metastasis breast cancer model (n=6, error bars for ±SD), the relative concentration: DOX 3 mg/kg, NFX 5 mg/kg. (a) Mean lung metastasis nodules of each group, (b) body weight shift along with the treatment days. ***p < 0.001 comparing to PBS group, (c) inhibition of metastasis by CLM from visualized lung metastatic nodules with yellow circles.

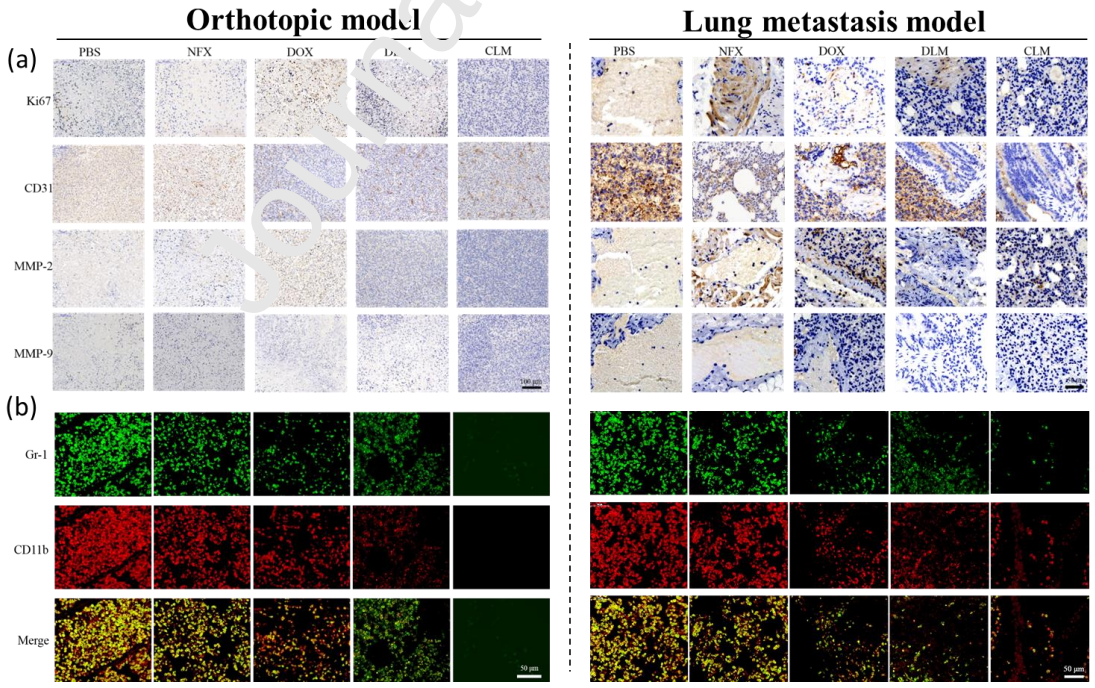

Figure 7. (a) Tumor apoptosis, proliferation, invasion and metastasis evaluated by Ki67, CD31, MMP-2 and MMP-9 IHC staining of tumors in mammary fat pad of orthotopic model (left panel) and pulmonary section in lung metastasis model (right panel), (b) double staining of anti-Gr-1 and

anti-CD11b antibodies on lung cord sections from both models for evaluating myeloid derived suppressor cells infiltration.

Graphical abstract

A cathepsin B/pH dual-sensitive block copolymer with doxorubicin was prepared to load nifuroxazide. The stimuli-responsive co-prodrug-loaded micelles showed great potential safe and efficient nanomedicine against breast cancer metastasis.

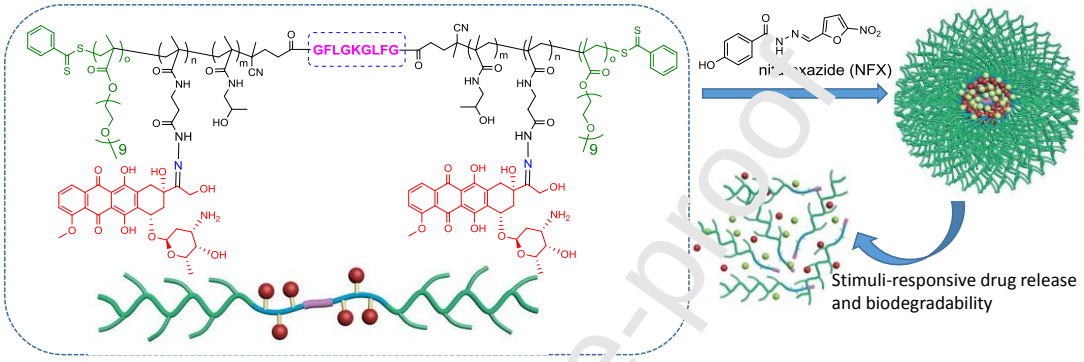

dfdfdf